Available online at www.sciencedirect.com
ScienceDirect
Polymer 48 (2007) 58–67
polymer
www.elsevier.com/locate/polymer

Grafting of hydrocarbon moieties on smectites by cold acetylene plasma and characterization of plasma-treated clay mineral polyethylene nanocomposites

Natacha Célini [a,b], Faiza Bergaya [b], Fabienne Poncin-Epaillard [a,*]

[a] Laboratoire Polymères Colloïdes et Interfaces (PCI), UMR-CNRS 6120, Université du Maine, Avenue Olivier Messiaen, 72 085 Le Mans Cedex 9, France
[b] Centre de Recherche sur la Matière Divisée (CRMD), UMR-CNRS 6619, Université d'Orléans, 1 bis rue de la Férollerie, 45 071 Orléans Cedex 2, France

Received 23 June 2006; received in revised form 10 October 2006; accepted 4 November 2006
Available online 29 November 2006

Abstract

The hydrophilic surface of montmorillonite and Laponite was changed to hydrophobic by treating the smectites with cold acetylene plasma, thus improving their compatibilization with polyethylene. The effects of plasma-polymerization on the clay minerals were studied by XRD, Raman and FTIR spectroscopies. The plasma treatment forms a coating on their external surfaces and also alters their structures, with a lesser effect on Laponite. The addition of these modified fillers to molten polyethylene leads to a decrease in the peak heat release rate.

Keywords: Plasma-polymerization; Acetylene; Clay minerals

1. Introduction

In the field of polymer composites, a new class of materials, the so-called nanocomposites, is being developed. This new class is composed of a polymer matrix and a filler of either natural or synthetic mineral particles. One of the most important forms of these hybrid organic–inorganic nanocomposites [1–5] is composed of layered silicates dispersed in the polymer matrix. These nanocomposites have attracted great interest, both in industry and in academia, because they often exhibit remarkable improvement in the characteristics of the material, such as better mechanical [6,7], ionic conductivity [8,9] or permeability properties [10].

The common layered silicates used in the nanocomposites belong to the general family of 2:1 phyllosilicates (Fig. 1). Each individual layer is composed of one alumina–oxygen–hydroxy octahedral sheet sandwiched between two identical silica–oxygen–tetrahedral sheets [11]. The layer thickness is about 1 nm, and its lateral dimension may vary from 30 nm to few micrometers, depending on the layered silicate. Isomorphic substitution within the layers (for example, Al^{3+} replaced by Mg^{2+} or Fe^{2+}, or Mg^{2+} replaced by Li^{+}) generates negative charges counterbalanced by alkali and alkaline earth cations, called exchangeable cations and located inside the interlamellar space.

Although the high aspect ratio of silicate nanolayers is ideal for reinforcement, the nanolayers are not easily dispersed in most polymers. Dispersion is further hindered by the intrinsic incompatibility of hydrophilic layered silicates and hydrophobic macromolecules [1,2]. Generally, the clay mineral is modified with an alkyl ammonium or phosphonium surfactant. Its affinity with the polymer is then stronger, since the surfactant adsorption leads to a more organophilic and less hydrophilic clay mineral surface [12,13].

This synthesis of the organoclay is run in wet organic or aqueous media with all the consequent problems relative to environmental protection associated with such a synthesis route. To avoid this wet chemistry, we propose an alternative route, the dry plasma technique which is able to alter the hydrophilic character of the clay mineral. The active species resulting from the glow discharge may etch, sputter, or be

* Corresponding author. Tel.: +33 2 43833978; fax: +33 2 43833558.
E-mail address: fabienne.poncin-epaillard@univ-lemans.fr (F. Poncin-Epaillard).

0032-3861/$ - see front matter © 2006 Elsevier Ltd. All rights reserved.
doi:10.1016/j.polymer.2006.11.018

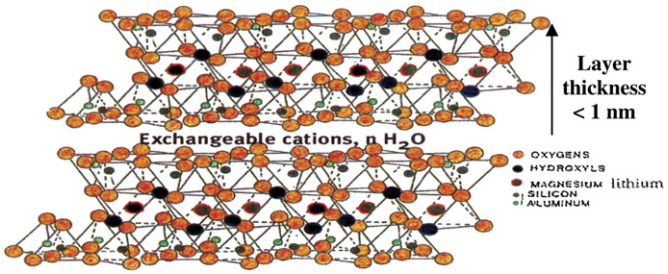

Fig. 1. Structure of the 2:1 clay mineral (Laponite).

deposited onto the substrate surface [14–18]. Recently, carbon black [19] was covered by plasma–polymer of styrene or butadiene. The tensile strengths and percent elongations of the final carbon black reinforced styrene butadiene rubber (SBR) vulcanizates are found to respond differently if modified fillers are used as compared with those prepared with unmodified fillers. Glass transition temperatures of vulcanizates are found to correlate well with the results of mechanical properties. Nah et al. [20] also showed that the surface modification of silica by the plasma-polymerization of acetylene leads to the formation of hydrocarbon layers mostly composed of C=C and C–H. The plasma-treated silica dispersion seemed to be dependent on the plasma parameters: short duration and low discharge power greatly improved the dispersion of the silica particles in SBR vulcanizates. The plasma modification of silica also improved the tensile modulus of SBR vulcanizates without deterioration of important basic properties such as tensile strength and elongation at break. However, no information was given on the structural morphology of the plasma-treated silica and of the blend at particle scale.

In this study, a radio-frequency (RF) glow discharge in acetylene was generated under reduced pressure and the plasma–polymer layered structure formed on the clay mineral was characterized. In a previous paper [21], the plasma parameters (treatment time t, discharge power P and acetylene flow Q) optimized in order to obtain the most hydrophobic coating onto model silicon wafer were detailed. These parameter conditions were: $t = 1$ min, $P = 20$ W and $Q_{C_2H_2} = 30$ sccm. The plasma–polymer structure was also characterized by Fourier transform infrared (FTIR) and X-ray photoelectron (XPS) spectroscopies. The coating was mostly composed of CH, CH_2, CH_3 groups, double carbon–carbon bonds and few oxygen–carbon bonds, corresponding to a hydrophobic material with a total surface energy of about 45 mJ m^{-2} and very weak polar component of about 4 mJ m^{-2}. Two clay minerals with different structures: natural montmorillonite from Wyoming (Na-Mt) and synthetic Na-Laponite RD (Na-Lp), were treated under these optimized conditions. The plasma-modified clay mineral was characterized by FTIR, Raman, XPS, X-ray diffraction (XRD) analyses and by transmission electron microscopic (TEM) observations. Finally, the plasma-treated clay minerals were incorporated into the polyethylene matrix. The thermal and mechanical properties of polyethylene–plasma-treated clay mineral nanocomposites are described.

2. Experimental part

2.1. Plasma chamber

This capacitive coupled RF reactor (Fig. 2) is devoted to the treatment of powder materials, such as clay minerals. The excitation module was a RF generator at 13.56 MHz (Sairem 0-600W), with a matching box adjusting the generator impedance to limit the reflected power. The reactor was a 310 mm × 255 mm rectangular aluminum chamber with its cathode linked to the generator and the anode grounded. Two quartz windows allowed optical examination. The pumping stage was composed of a primary pump (CIT-ALCATEL N°2010 SD) and a turbomolecular pump (ALCATEL ATP 80/100). The pressure was measured with a Pirani gauge (ACC 1009). Mass flowmeters (Aera FC 7700 CDC) controlled the amount of injected gas. The distance between the sample and the cathode was 120 mm. A vibrating plate (180 mm length, 120 mm width and 14 mm height) guaranteed a homogeneous mixing of the clay mineral during the plasma treatment. Different vibration frequencies (f from 0 to 270 a.u. (arbitrary units)) could be applied during the treatment of the clay minerals. Before turning on the discharge, the clay mineral sample (2 g) was spread on the plate by vibrating during 2 min at $f = 100$ a.u. The plasma-polymerization and deposition onto the particles were studied as a function of the mechanical stirring.

2.2. Materials

High purity acetylene (C_2H_2, 99.95%) was obtained from Air Liquide.

Natural montmorillonite of Wyoming (Na-Mt), a dioctahedral 2:1 clay mineral, was provided by the Comptoir des Minéraux et Matières Premières (France). It was used as received without further purification.

Synthetic Na-Laponite RD (Na-Lp), a trioctahedral 2:1 clay mineral, was purchased from Laporte Ltd. Its chemical formula is $(Si_{7.98}Al_{0.02})(Mg_{5.44}Li_{0.40})O_{20}(OH)_4(Na_{0.74}Ca_{0.03})$ and it was used as received without further treatment.

The linear low-density polyethylene (LLDPE, Exxon, density = 0.918 g cm^{-3}, crystallinity = 43%) was used as polymer matrix.

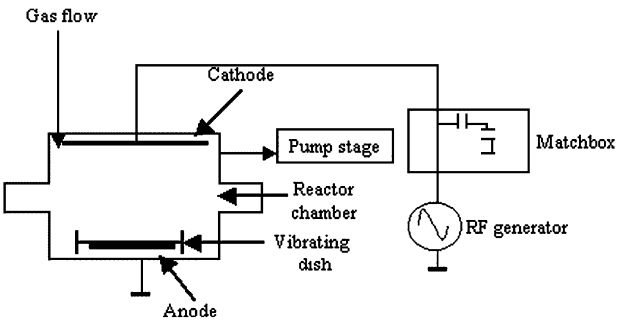

Fig. 2. Schematic diagram of the plasma reactor.

The nanocomposites were obtained by compounding the molten polymer with 5% of plasma-treated clay mineral in a Brabender internal mixer (370 cm^3) at 30 rpm for 15 min.

2.3. FTIR, Raman, XPS, XDR and TEM techniques

FTIR spectra were recorded by means of a Bruker IFS 66 spectrophotometer. The spectrum of each sample was recorded in triplicate by accumulating 100 scans at 4 cm^{-1} resolution between 7000 and 400 cm^{-1}. The sample was prepared by mixing KBr powder (99 mg) and plasma-treated clay mineral (1 mg).

Raman spectroscopy was performed on a Jobin–Yvon T64000 spectrometer with the B×40 Olympus microscope at the Laboratoire de Physique de l'Etat Condensé (Université du Maine, Le Mans). The Na-Lp disk spectra were recorded at 514.5 nm line from a spectrum coherent Ar/Kr laser with 30 mW excitation power on the sample and three accumulations at 100 s integration time. The laser spot focused on the sample was approximately 2 μm in diameter. Because of the phenomenon of fluorescence emitted by Na-Mt, exploitable Raman spectra of this clay mineral could not be obtained [22].

XPS spectra are acquired on an Escalab VG220 ESCA instrument. The photo-emission was excited by a monochromatic Mg Kα beam at 1253.6 eV. All spectra are referenced to the C_{1s} peak for carbon at 285 eV. Peak fitting was done using Peak fit software (version 4.0 Jandel).

The XRD spectra (Cu Kα radiation at 40 kV/30 mA) of the clay minerals were collected at room temperature on a Θ–Θ diffractometer equipped with an intrinsic germanium detector system (Phillips PW 1830).

The TEM used was a Phillips CM 20 instrument using an accelerating voltage of 100 kV. The pictures recorded correspond to clay mineral molded in acrylic resin. The clay mineral was dispersed in alcohol solution under ultrasonic stirring, and a drop of this suspension was placed in a mold and then dried. The deposit layered with an acrylic resin (LR White) was dried under vacuum (maximum pressure = 2 bars) overnight. The resin containing clay mineral was microtomed with a diamond knife (Drubber) in a direction normal to the plane of the deposit.

2.4. Combustion experiments and mechanical property measures of the composite

Combustion experiments and mechanical property measurements were carried out at the Centre de Recherche de Nexans (Lyon, France). Combustion experiments were performed on full-blown variety marketed by fire testing technology in an oxygen consumption calorimeter at an incident heat flux of 30 kW/m^2. HRR (heat release rate), PHRR (peak heat release rate), extinction time and inflammation time data are collected. The cone data reported here were averaged on three replicated experiments. The mechanical measurements performed on a traction machine (type ZWICK 1010) were run with H_2 test tubes, cut up on a specimen (1 mm of thickness).

3. Results and discussion

3.1. Chemical structure of the plasma-treated clay minerals

Both clay minerals were treated under the optimum parameters [21] of the plasma-polymerization ($P = 20$ W, $Q_{C_2H_2}$ = 30 sccm and $t = 1$ min) in function of the mechanical stirring f. The FTIR spectra (Figs. 3 and 4) of these plasma-treated clay minerals present some peak alterations depending on

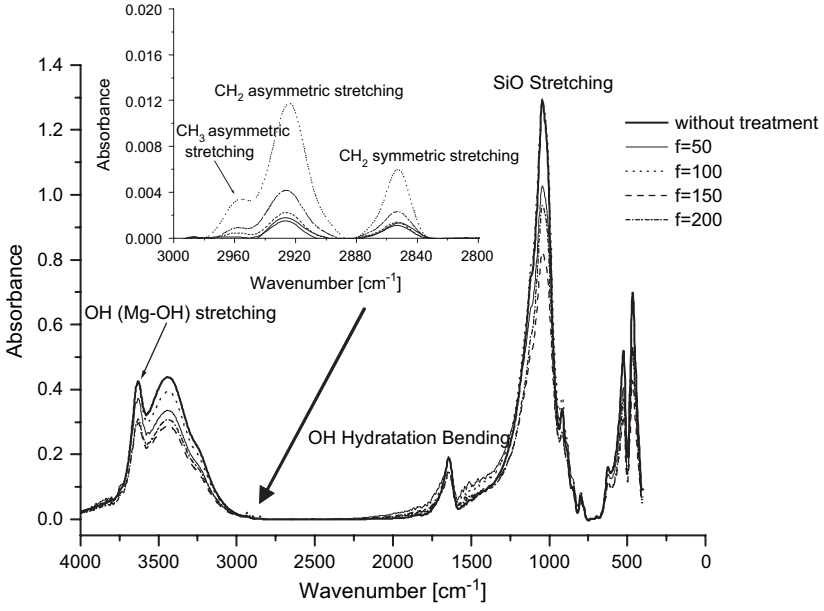

Fig. 3. FTIR spectra of the virgin and the plasma-treated Na-Mt ($P = 20$ W, $Q_{C_2H_2}$ = 30 sccm and $t = 1$ min) for different mechanical stirring f.

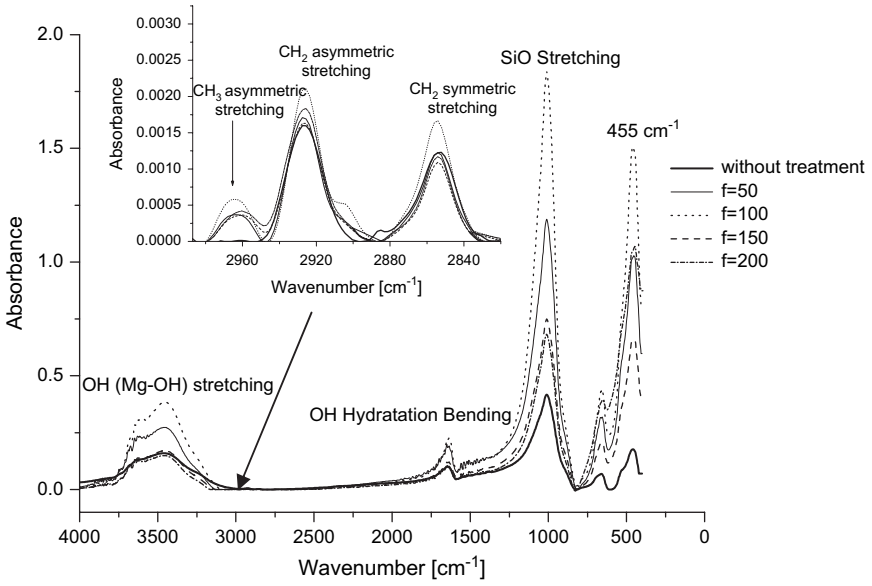

Fig. 4. FTIR spectra of the virgin and the plasma-treated Na-Lp ($P = 20$ W, $Q_{C_2H_2} = 30$ sccm and $t = 1$ min) for different mechanical stirring f.

the mechanical friction. The intensity of the SiO stretching vibration peak of Na-Mt and Na-Lp, respectively, at 1043 and 1011 cm^{-1}, the OH stretching vibration peak of both clay minerals in the range of 3000–3800 cm^{-1} and the OH bending vibration peak of absorbed water (Na-Mt: 1648 cm^{-1}, Na-Lp: 1633 cm^{-1}) are modified after the plasma treatment, whatever the value of the stirring amplitude.

The intensity of SiO peak of Na-Mt decreases randomly with the mechanical stirring. This variation emphasizes the modification of the environment of tetrahedral sites SiO_4 [23]. The small diminution of the OH peak intensities corresponding to the absorbed water and Mg–OH bond illustrates a small dehydration and dehydroxylation of the clay mineral.

An opposite evolution of the plasma-treated Na-Lp FTIR signature is noticed: the intensities of the hydroxyl and SiO groups increase randomly with the mechanical stirring.

The acetylene plasma treatment leads to the grafting of alkyl groups, as shown by the presence of a shoulder at 2963 cm^{-1} (CH_3 asymmetric stretching) and two peaks at 2925 cm^{-1} (CH_2 asymmetric stretching) and 2854 cm^{-1} (CH_2 symmetric stretching), even if the presence of hydrocarbon contamination of virgin clay minerals is noticed. The intensity of these small absorbance peaks depends on the mechanical stirring.

By determining the ratio of the intensities of the alkyl (2925 cm^{-1}) and the MgOH (3630 cm^{-1}) peaks (Fig. 5), we noted that the density of alkyl groups for both clay minerals increases with the mechanical friction. There are more alkyl functions present on the Na-Mt particles than on the Na-Lp particle, depending probably on the size of the clay mineral particles. Indeed, the Na-Mt particle is composed of layers with a length of 1 μm whereas the Na-Lp particle has a smaller lateral extension between 20 and 30 nm [11]. The deposition and the grafting of hydrocarbon therefore depend on the morphological structure of the clay mineral. Besides, the forces of friction induced by the strong stirring should limit the coating on Na-Mt while mechanical stirring has a lesser effect on the alkyl groups' density of Na-Lp.

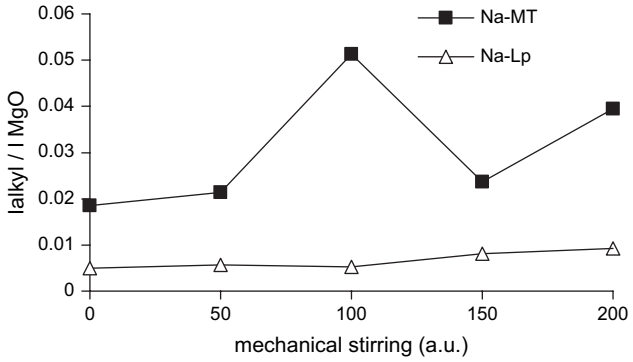

Fig. 5. Variation of the ratio between the intensities of the alkyl (2925 cm^{-1}) and the MgOH (3630 cm^{-1}) peaks of the plasma-treated Na-Mt and Na-Lp versus the mechanical stirring f ($P = 20$ W, $Q_{C_2H_2} = 30$ sccm and $t = 1$ min).

Raman spectra of the plasma-treated Na-Lp at $f = 150$ a.u. (Fig. 6) show that the plasma alters the tetrahedral sites SiO_4 of this clay mineral. The vibration modes of SiO_4 are modified after the treatment. The peak at 689 cm^{-1} is shifted by 8 cm^{-1} towards smaller wavenumbers and the peaks at 1030, 332 and 731 cm^{-1} vanish. The disappearance of these peaks is probably due to the bombardment of the clay mineral surface by energetic electrons. The plasma treatment also modifies the oxygen of the octahedral layer, since the peak at 285 cm^{-1} is shifted towards higher wavenumbers. The Mg sites of octahedral layers of Na-Lp seem to be unaltered by the plasma treatment, both vibration modes at 108 and 185 cm^{-1} remaining unchanged. These results were confirmed by XPS analyses.

From the decomposition of the O_{1s} high-resolution peak, the variation of the SiO and MgO chemical bond densities

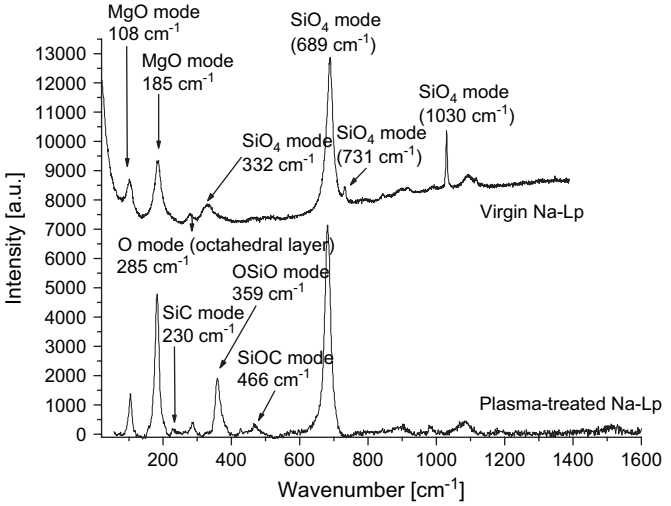

Fig. 6. Raman spectrum of the virgin and the plasma-treated Na-Lp ($P = 20$ W, $Q_{C_2H_2} = 30$ sccm, $t = 1$ min and $f = 150$ a.u.).

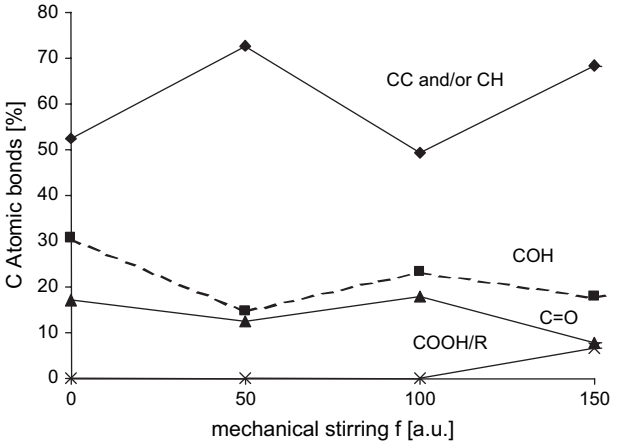

Fig. 8. Variation of $C-C$ and/or $C-H$, $C-OH$, $C=O$ and $C-OOH/R$ bond densities of the plasma-treated Na-Lp versus the mechanical stirring f ($P = 20$ W, $Q_{C_2H_2} = 30$ sccm and $t = 1$ min). $f = 0$ a.u. corresponds to the virgin Na-Lp.

versus mechanical stirring is presented in Fig. 7. Even with low mechanical stirring, the SiO bonds are degraded. At $f = 100$ a.u., Na-Lp only contains 31.2% of SiO bonds as against 33.7% for the blank sample. The Si–O bonds seem to be highly sensitive either to the plasma species bombardment or to the mechanical friction induced by the stirring. The degradation of MgO bonds in the octahedral layer is much more limited. The proportion of MgO bonds in the pristine sample is 4.1%. After treatment, this value remains almost constant for all the vibration frequencies. The formation of new bonds such as SiC (230 cm^{-1}), SiOC (427 and 466 cm^{-1}) and OSiO (359 cm^{-1}) [24,25] are evidenced by Raman spectroscopy. These results could indicate that the coating is bonded to the silicon atoms of the clay mineral. The decomposition of the C_{1s} high-resolution peak gives four environmental types: $C-C$ and/or $C-H$, $C-OH$, $C=O$ and $C-OOH/R$. The evolution of the percentage of these species versus the mechanical stirring (Fig. 8) shows that the hydrocarbon coating is constituted mostly of $C-C$ and/or $C-H$ around 68%, 18% of $C-OH$, 8% of $C=O$ and 6% of $C-OOH/R$.

3.2. Structure of the plasma-treated clay minerals

The X-ray diffractograms (Fig. 9) show that the plasma treatment destroys the morphological structure of Na-Mt. After the treatment, the basal distance d_{001} is linearly shifted to lower values depending on the mechanical stirring until $f = 150$ a.u. (Fig. 10). The d_{001} of the pristine clay mineral is 1.26 nm as against 0.99 nm for the treated sample (at $f = 150$ a.u.). The d_{001} decrease is probably due to the loss of water molecules of the hydrated layer of the exchangeable cations. From this result, we may suppose that the coating is bonded to the external layer of Na-Mt. The intensity maximum also decreases probably due to the decrease of the coherence domain. The shape of this peak is also modified with the expansion of the latter. This modification shows and confirms the dehydroxylation of Na-Mt after the plasma treatment.

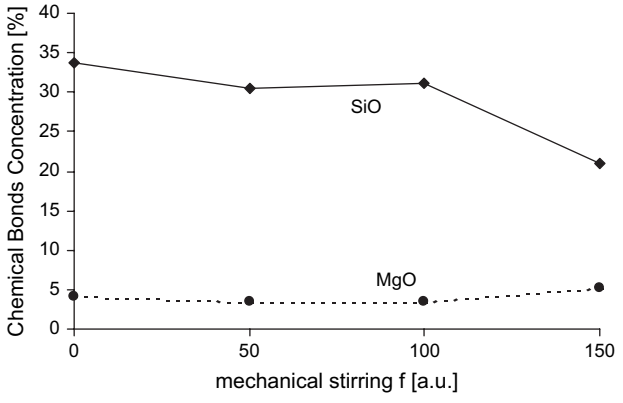

Fig. 7. Variation of SiO and MgO chemical bond densities versus the mechanical stirring f for the plasma-treated Na-Lp ($P = 20$ W, $Q_{C_2H_2} = 30$ sccm and $t = 1$ min). $f = 0$ a.u. corresponds to the virgin Na-Lp.

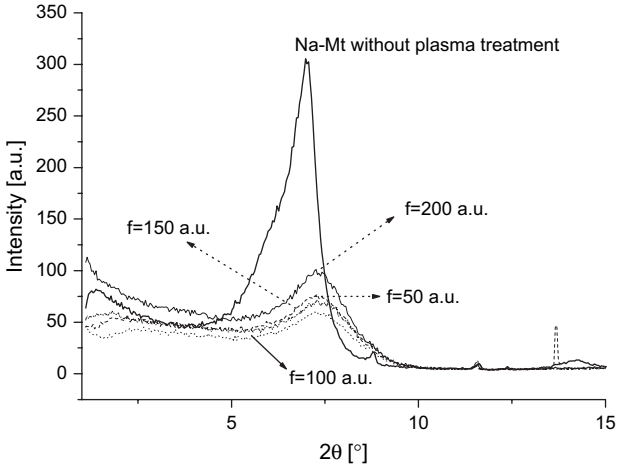

Fig. 9. XRD spectra of the virgin and plasma-treated Na-Mt ($P = 20$ W, $Q_{C_2H_2} = 30$ sccm and $t = 1$ min) at different mechanical stirring f.

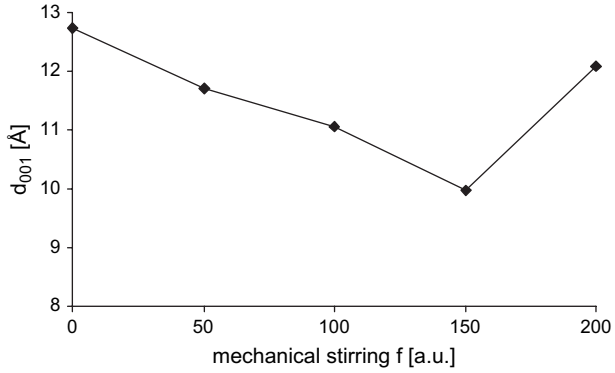

Fig. 10. Evolution of the d_{001} basal distance of the plasma-treated Na-Mt ($P = 20$ W, $Q_{C_2H_2} = 30$ sccm and $t = 1$ min) versus the mechanical stirring f.

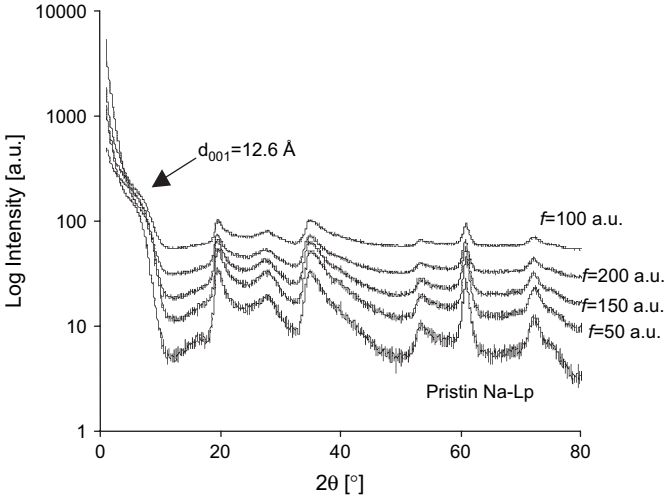

Fig. 11. XRD spectra of the virgin and plasma-treated Na-Lp ($P = 20$ W, $Q_{C_2H_2} = 30$ sccm and $t = 1$ min) at different mechanical stirring f.

Na-Lp has a different behavior. The structure of this clay mineral is not altered by the treatment (Fig. 11). Indeed, the shoulder centered at 1.26 nm remains unchanged, whatever the mechanical stirring. Again, since this parameter is unchanged, it seems likely that the coating is fixed onto the external surface of Na-Lp.

The TEM image of the pristine Na-Mt shows an ensemble of flexible ribbons (Fig. 12a). Each ribbon, corresponding to one layer, has an approximate length of 1 μm and a thickness of 1 nm. The plasma treatment of Na-Mt induces the formation of clay mineral particles with a more important number of layers per particle (Fig. 12b) and with the appearance of column defects. In some zones, the clay mineral seems to be perturbed, probably by the dehydroxylation of the clay mineral. This phenomenon is emphasized by the presence of holes in the structure of the clay mineral. The presence of these holes decreases the coherence domain, explaining and confirming the decrease of the d_{001} peak intensity.

The Na-Lp structure is different from that of Na-Mt. It appears as an ensemble of isolated particles composed of thin layers. Each layer has a lateral extension between 20 and 30 nm and a thickness of 1 nm (Fig. 13a). Although the peak d_{001} remains unchanged, the arrangement of layers seems to be altered (Fig. 13b). The particles are constituted of five layers on an average. However, the distribution of the stacking sizes is rather heterogeneous. Moreover, the TEM of the

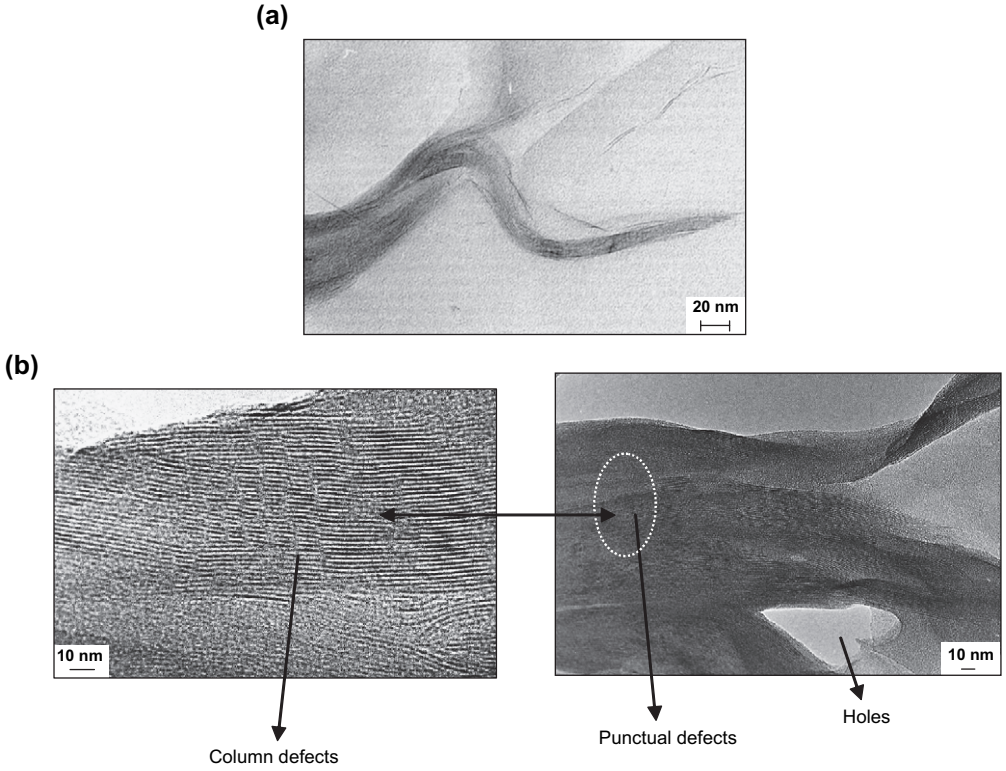

Fig. 12. Transmission electron micrographs of: (a) the blank Na-Mt and (b) the plasma-treated Na-Mt ($P = 20$ W, $Q_{C_2H_2} = 30$ sccm, $t = 1$ min and $f = 150$ a.u.).

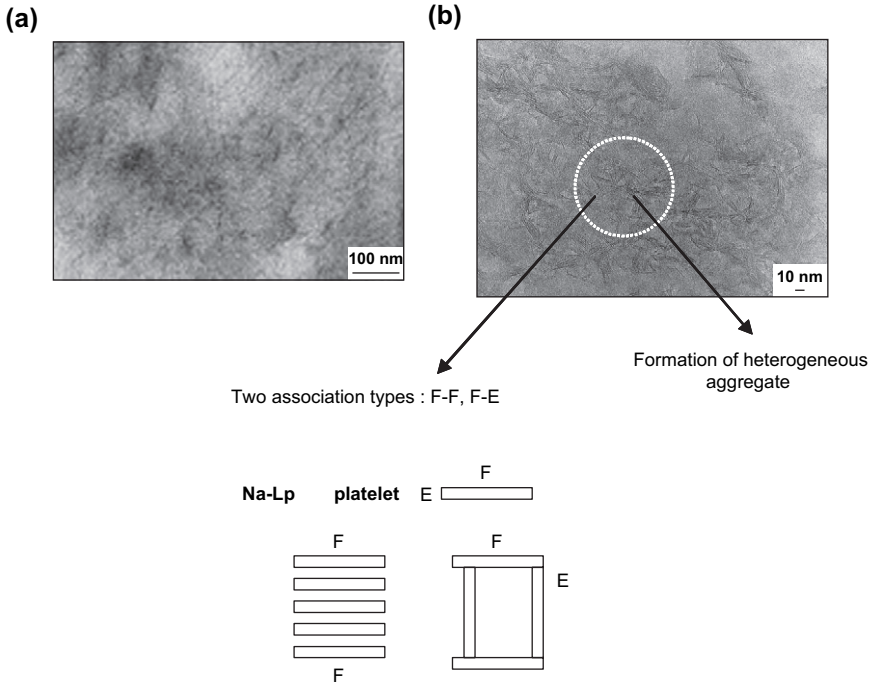

Fig. 13. Transmission electron micrographs of: (a) the blank Na-Lp, (b) the plasma-treated Na-Lp ($P = 20$ W, $Q_{C_2H_2} = 30$ sccm, $t = 1$ min and $f = 150$ a.u.).

plasma-treated Na-Lp shows two types of associations: face–face (F–F) and face–edge (F–E). After the treatment, the size of the layers remains unchanged.

In our previous paper [21], we observed a different behavior of the adsorption properties of plasma-treated clay minerals: the plasma-treated Na-Mt seems to be more hydrophilic and the plasma-treated Na-Lp more hydrophobic. The difference in behavior can be explained qualitatively by the different textures between these two clay minerals. The effect of the plasma on Na-Mt leads to scission of the SiO bonds (on the external surfaces) and grafting of the alkyl groups. Moreover, Na-Mt is composed of stacked layers that form particles with large lateral extension. Following the bombardment by the species in the plasma phase (radicals, electrons and ions), one can imagine the scission of some SiO bonds without the grafting of alkyl groups, with the creation of new polar sites. The surface of the plasma-treated Na-Mt becomes more hydrophilic, as compared to the non-treated Na-Mt. The anisotropy of Na-Lp is less important; the platelets are smaller and more delaminated, and therefore more accessible to the plasma phase. The difference in behavior can also be assigned to the tortuosity of the diiodomethane path. The presence of holes and column defects in the clay mineral structure increases the time required to wet completely the powder bed, as found with the Na-Mt particles.

3.3. Flammability properties of plasma-treated clay mineral polyethylene nanocomposites

Characterization of the flammability properties of a variety of clay mineral–polymer nanocomposites, under fire-like conditions, using the cone calorimeter, has revealed improved flammability properties for many types of clay–polymer nanocomposites [26,27]. The cone calorimeter is one of the most effective bench-scale methods for studying the flammability properties of materials. Heat release rate (HRR) and, more particularly peak HRR have been found to be the most important parameters in the evaluation of fire safety [26]. The cone calorimeter data show that both peak and average HRR were reduced significantly for nanocomposites with low clay mineral mass fraction (2–5%) [26].

Plasma-treated clay mineral particles were mixed with the polyethylene matrix (5% mass fraction). Characterization of the flammability properties of plasma-treated Na-Mt polyethylene nanocomposites is presented in Table 1. The inflammation and extinction times, the HRR and the peak HRR are modified. After the addition of plasma-treated Na-Mt, the polyethylene catches fire more rapidly. For example, when 5% of Na-Mt treated at $f = 50$ a.u. is mixed with the polyethylene, the polymer burns after 107 s against 137 s (without any filler). It burns by releasing an HRR weaker, compared to those of polymer alone. By following the variation of HRR versus time (Fig. 14), we note that the shape of the polyethylene peak is modified after the addition of the plasma-treated Na-Mt. The degradation kinetic of the polyethylene is modified. The addition of plasma-treated Na-Mt decreases the peak HRR intensity. A minimum value (31%) is obtained with a Na-Mt treated by a mechanical stirring of 50 a.u. The peak HRR is equal to 554 KW/m^2 against 803 kW/m^2 for the pristine polyethylene. Even if taking into account the error bar of such measurement, the peak HRR is decreasing; the mass loss is slightly increasing when adding plasma-treated Na-Mt to PE and its value is slightly dependent on the stirring.

Table 1
Cone calorimeter data of polyethylene (PE) and polyethylene/(5%) plasma-treated Na-Mt nanocomposites ($P = 20$ W, $Q_{C_2H_2} = 30$ sccm and $t = 1$ min; incident heat flux of 30 kW/m^2) for different mechanical stirring (f)

Composition	Inflammation time (s)	Extinction time (s)	Heat release rate average (kW/m^2)	Peak heat release rate (kW/m^2, %)	Mass loss rate (%)
PE	137	668	208	803 ± 10	–
PE + plasma-treated Na-Mt ($f = 50$ a.u.)	107	789	117	554 ± 10	76
PE + plasma-treated Na-Mt ($f = 100$ a.u.)	101	609	139	575 ± 10	77
PE + plasma-treated Na-Mt ($f = 150$ a.u.)	109	854	133	679 ± 10	83
PE + plasma-treated Na-Mt ($f = 200$ a.u.)	112	797	122	665 ± 10	82

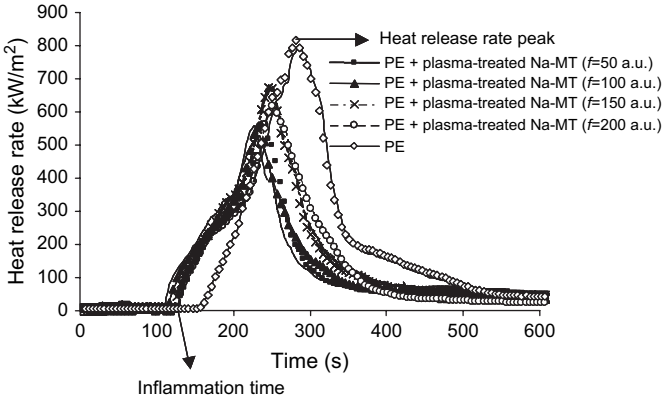

Fig. 14. Heat release rate (HRR, incident heat flux of 30 kW/m^2) data for pure PE and their polyethylene/(5%) plasma-treated Na-Mt nanocomposites ($P = 20$ W, $Q_{C_2H_2} = 30$ sccm and $t = 1$ min) for different mechanical stirring (f).

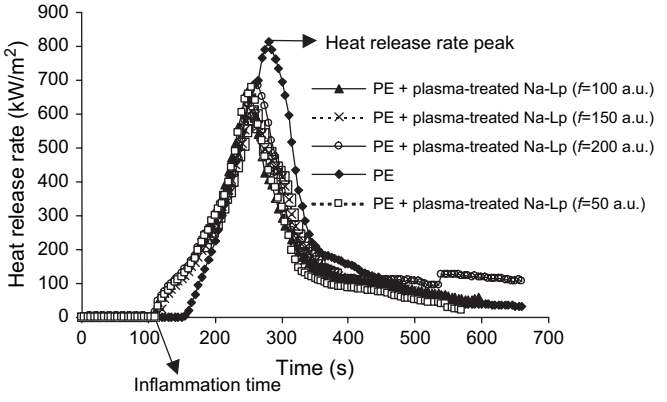

Fig. 15. Heat release rate (HRR, incident heat flux of 30 kW/m^2) data for pure PE and their polyethylene/(5%) plasma-treated Na-Lp nanocomposites ($P = 20$ W, $Q_{C_2H_2} = 30$ sccm and $t = 1$ min) for different mechanical stirring (f).

As for the plasma-treated Na-Mt, the addition of Na-Lp modifies the polyethylene behavior: the inflammation time is accelerated and the extinction time is diminished (Table 2). The shape of the peak HRR and therefore the degradation kinetic are weakly modified (Fig. 15). The peak HRR is weakly diminished and is minimum for a mechanical vibration of 150 a.u. and the HRR is decreased by 22.7% and is equal to 621 kW/m^2.

3.4. Mechanical properties of plasma-treated clay mineral polyethylene nanocomposites

After the addition of plasma-treated Na-Mt, the mechanical properties of the PE are weakly modified (Table 3). Indeed, the elongation at break and the strain at break weakly decrease. However, the Young's modulus increases after the addition of the plasma-treated Na-Mt. The addition of the plasma-treated Na-Lp weakens the mechanical properties of the polyethylene: the elongation at break and the strain at break are hardly degraded (Table 4). With the plasma-treated Na-Lp at $f = 50$ a.u., the strain at break goes through 19.8 to 15.2 MPa and the elongation at break decreases from 798% for the polyethylene alone to 664% for plasma-treated Na-Lp. Na-Mt treated by C_2H_2 plasma gives a good compromise between a non-negligible decrease of peak HRR and a weak alteration of the polyethylene mechanical properties. When Mt modified with an alkyl ammonium (5 wt%) is added to the molten high-density polyethylene (HDPE) [28], the peak HRR of such a nanocomposite decreases by 32% as compared

Table 2
Cone calorimeter data of polyethylene (PE) and polyethylene/(5%) plasma-treated Na-Lp nanocomposites ($P = 20$ W, $Q_{C_2H_2} = 30$ sccm and $t = 1$ min; incident heat flux of 30 kW/m^2) for different mechanical stirring (f)

Composition	Inflammation time (s)	Extinction time (s)	Heat release rate average (kW/m^2)	Peak heat release rate (kW/m^2, %)
PE	137	668	208	803 ± 10
PE + plasma-treated Na-Lp ($f = 50$ a.u.)	98	628	187	628 ± 10
PE + plasma-treated Na-Lp ($f = 100$ a.u.)	105	603	198	671 ± 10
PE + plasma-treated Na-Lp ($f = 150$ a.u.)	95	578	194	621 ± 10
PE + plasma-treated Na-Lp ($f = 200$ a.u.)	104	553	199	722 ± 10

Table 3
Mechanical properties of polyethylene (PE) and their polyethylene/(5%) plasma-treated Na-Mt nanocomposites ($P = 20$ W, $Q_{C_2H_2} = 30$ sccm and $t = 1$ min) for different mechanical stirring (f)

Composition	Strain at break (MPa)	Elongation at break (%)	Module de Young (N/mm^2)
PE	19.8	798	144
PE + plasma-treated Na-Mt ($f = 50$ a.u.)	17.4	737	188
PE + plasma-treated Na-Mt ($f = 100$ a.u.)	17.5	745	180
PE + plasma-treated Na-Mt ($f = 150$ a.u.)	17.6	725	185
PE + plasma-treated Na-Mt ($f = 200$ a.u.)	17.2	718	195

Table 4
Mechanical properties of polyethylene (PE) and their polyethylene/(5%) plasma-treated Na-Lp nanocomposites ($P = 20$ W, $Q_{C_2H_2} = 30$ sccm and $t = 1$ min) for different mechanical stirring (f)

Composition	Strain at break (MPa)	Elongation at break (%)	Module de Young (N/mm^2)
PE	19.8	798	144
PE + plasma-treated Na-Lp ($f = 50$ a.u.)	15.2	664	171
PE + plasma-treated Na-Lp ($f = 100$ a.u.)	15.2	661	169
PE + plasma-treated Na-Lp ($f = 150$ a.u.)	15.1	649	195
PE + plasma-treated Na-Lp ($f = 200$ a.u.)	15.4	673	160

to that of pure HDPE. The peak HRR diminution obtained with Na-Mt treated with the acetylene plasma is comparable (31%) to those obtained by Wang et al. [31]. From these preliminary results, the formation of a nanocomposite could be expected. When the polymer nanocomposite with a filler as Na-Mt modified with alkyl ammonium surfactant burns, a plateau due to its charring is observed. The charring can serve as a barrier to both mass and energy transport. This effect is linked to the nanodispersion of the clay mineral in the polymer matrix [27,29,30]. Here, the plateau is not reached probably because the dispersion is not efficiently homogeneous, with the presence of intercalated layers and probably aggregates in the matrix polymer [31,32]. With Na-Lp, we obtained the formation of a composite where the polymer matrix is not inserted between the layers but is forming separate aggregates.

4. Conclusion

Two clay minerals with different aspect ratios and structural arrangements have been modified by acetylene cold plasma treatment. The plasma treatment has two effects on the clay mineral surface: (i) the modification of the SiO_4 environment and (ii) the grafting of hydrocarbon groups. The coating, essentially constituted of CH_2 and CH_3 groups, is effectively on the external surface of the clay mineral owing to the attack of the silicon sites. The coating thickness, depending on the structure of the clay mineral, has been optimized for different plasma parameters. The plasma treatment has also both side effects: the dehydration and the dehydroxylation of the clay mineral associated with the SiO_4 alteration. The plasma treatment modifies Na-Mt, leading to the formation of holes and column defects in the structure. The plasma-treated Na-Mt becomes more hydrophilic, whereas, the plasma treatment of Na-Lp leads to the rebuilding of the structure, with the clay mineral becoming hydrophobic after the plasma treatment. Therefore, one can assume that besides the coating deposition, this alteration is induced not only by a physical phenomenon, ionic bombardment, but also by the chemical one that corresponds to dehydration and dehydroxylation of the clay mineral both leading to the scission of SiO bonds.

The addition of plasma-treated clay minerals as fillers in the polyethylene matrix decreases the flammability but degrades the mechanical properties of the clay mineral polymer nanocomposites. The best compromise is obtained with Na-Mt treated by acetylene plasma where the mechanical properties are less degraded and the heat release rate decreases by about one-third compared to the pristine polyethylene.

Acknowledgments

This project is financially sponsored by MINEFI and we are grateful for their support. This work is a part of a project between CRMD (Orléans), PCI (Le Mans), Pharmacie Centrale de France (La Voûlte sur Rhônes) and Nexans (NRC-Lyon). We are thankful for CRT Plasma Laser (Orléans) coordinator of the project. The assistance of C. Clinard and T. Caciaguerra for obtaining the TEM images is gratefully acknowledged.

References

[1] Vaia RA, Giannelis EP. Macromolecules 1997;30:7990–9.
[2] Vaia RA, Giannelis EP. Macromolecules 1997;30:8000–9.
[3] Vaia RA, Ishii H, Giannelis EP. Chem Mater 1993;5:1694–6.
[4] Vaia RA, Jandt KD, Kramer EJ, Giannelis EP. Macromolecules 1995;28:8080–5.
[5] Vaia RA, Jandt KD, Kramer EJ, Giannelis EP. Chem Mater 1996;8:2628–35.
[6] Fornes TD, Yoon PJ, Keskkula H, Paul DR. Polymer 2001;42:9929–40.
[7] Hasegawa N, Kawasumi M, Kato M, Usiki A, Okada A. J Appl Polym Sci 1998;67:87–92.
[8] Aranda P, Ruiz-Hitzhy E. Appl Clay Sci 1999;15:119–35.
[9] Sandi G, Carrado KA, Joachin H, Lu W, Prakash J. J Power Sources 2003;119–121:492–6.
[10] Yano K, Usiki A, Okada A, Kurauchi T, Kamigaito O. J Polym Sci Part A Polym Chem 1993;31:2493–8.
[11] Grim RE. Clay mineralogy. 2nd ed. New York: McGraw-Hill; 1968.
[12] Wang KH, Choi MH, Koo CM, Choi YS, Chung IJ. Polymer 2001;42(24):9819–26.
[13] Heinemann J, Reichert P, Thomson R, Mulhaupt R. Macromol Rapid Commun 1999;20:423–30.
[14] d'Agostino R. Plasma deposition, treatment and etching polymers. New York: Academic Press; 1990.
[15] Yasuda H. Plasma polymerization, vol. 1. New York: Academic Press; 1985.
[16] Yasuda H. J Macromol Sci Chem 1976;A10(3):383–420.
[17] Yasuda H. Glow discharge polymerization. New York: Academic Press; 1978.
[18] Morosoff N. An introduction to plasma polymerization. New York: Academic Press; 1990.
[19] Akovali G, Ulkem I. Polymer 1999;40:7417–22.
[20] Nah C, Huh MY, Rhee JM, Yoon TH. Polym Int 2002;51:510–8.
[21] Le Dû G, Célini N, Bergaya F, Poncin-Epaillard F. Surf Coat Technol 2006, in press.
[22] Frost RL, Rintoul L. Appl Clay Sci 1996;11:171–83.
[23] Yariv S. Clays Miner 1986;21:925.
[24] During JR, Sullivan JF, Cox AW, Streusand BJ. Spectrochim Acta Part A 1978;34:719–30.
[25] Mondragon MA, Castano VM, Garcia JM, Tellez CAS. Vib Spectrosc 1995;9:293–304.
[26] Gilman JW. Appl Clay Sci 1999;15:31–49.

[27] Zanetti M, Kashiwagi T, Falqui L, Camino G. Chem Mater 2002;14: 881–7.
[28] Wang S, Hu Y, Zhongkai Q, Wang Z, Chen Z, Fan W. Mater Lett 2002; 4222:1–4.
[29] Zhu J, Morgan AB, Lamelas FJ, Wilkie CA. Chem Mater 2001;13: 3774–80.
[30] Manias E, Touny A, Wu L, Strawhecker K, Lu B, Chung TC. Chem Mater 2001;13:3516–23.
[31] Zanetti M, Camino G, Thomann R, Mülhaupt R. Polymer 2001;42: 4501–7.
[32] Zanetti M, Camino G, Mülhaupt R. Polym Degrad Stab 2001;74: 413–7.